Laser Physics Letters

LETTER

Coherent near-infrared light generation based on self-seeded parametric four-wave mixing in Rb vapor

To cite this article: Xuewen Wang *et al* 2021 *Laser Phys. Lett.* **18** 055207

IOP Publishing | Astro Ltd Laser Physics Letters
Laser Phys. Lett. **18** (2021) 055207 (5pp) https://doi.org/10.1088/1612-202X/abf5d1

Letter

Coherent near-infrared light generation based on self-seeded parametric four-wave mixing in Rb vapor

Xuewen Wang[1,2], Jinpeng Yuan[1,2,*], Lirong Wang[1,2,*], Liantuan Xiao[1,2] and Suotang Jia[1,2]

[1] State Key Laboratory of Quantum Optics and Quantum Optics Devices, Institute of Laser Spectroscopy, Shanxi University, 92 Wucheng Road, Taiyuan 030006, People's Republic of China
[2] Collaborative Innovation Center of Extreme Optics, Shanxi University, 92 Wucheng Road, Taiyuan 030006, People's Republic of China

E-mail: yjp@sxu.edu.cn and wlr@sxu.edu.cn

Received 19 January 2021
Accepted for publication 5 April 2021
Published 23 April 2021

Abstract

We demonstrate 1.37 μm coherent near-infrared light generation via self-seeded parametric four-wave mixing (FWM) process in Rb atomic vapor. Two lasers (780 nm and 776 nm) in the co-propagating configuration, drive the Rb atoms from the $5S_{1/2}$ ground state to the $5D_{5/2}$ excited state. The parametric FWM around the $5P_{3/2}$–$5D_{5/2}$–$6P_{3/2}$–$6S_{1/2}$–$5P_{3/2}$ transition loop is effectively established under phase matching conditions. The generated coherent light wavelength is confirmed using an optical spectrum analyzer, and the output power is investigated with the input laser frequency, power and atomic density. Consequently, a 1.37 μm coherent light with the power of 27 μW and the beam quality of $M_x^2 = 1.22$ and $M_y^2 = 1.25$ is obtained. An additional 795 nm laser is introduced to enhance the output power by 1.5 times through velocity-selective optical hyperfine repumping.

Keywords: coherent near-infrared light, four-wave mixing, amplified spontaneous emission

(Some figures may appear in color only in the online journal)

1. Introduction

Diode pumped alkali lasers (DPALs) are a new type of laser based on the excitation of alkali atomic vapors and play a crucial role in the laser invention [1]. These novel lasers combine the characteristics of both gas and solid-state lasers, and can be used as excellent substitutes of solid-state and chemical lasers owing to high quantum efficiency, high beam quality and better thermal management. High power DPALs can be used to charge remote photovoltaic cells and remote material processing [2], whereas moderate to low power DPALs with narrow linewidth are suitable for research in quantum optics [3, 4], optical communication [5] and atomic physics [6, 7].

DPALs are primarily produced by the nonlinear optical effects of parametric four-wave mixing (FWM) [8] and amplified spontaneous emission (ASE) [9]. FWM is a practical and effective technique for generating polychromatic optical fields with high coherence, tunable narrowband and high beam quality. Therefore, frequency conversion in atomic ensembles has been a very active research area in FWM process, which will result in the efficient generation of new coherent optical fields, expanding from ultraviolet (UV) [10] to infrared (IR) [11] via different atomic transitions. The UV or blue lasers are widely investigated in underwater optical communication [12], while the IR lasers promote the progress in laser guide star technique [13] and remote magnetometry [14, 15]. In particular, the IR lasers simultaneously match with a telecom window and an atomic transition line, thus they can be used to realize long-distance quantum networks [16].

* Authors to whom any correspondence should be addressed.

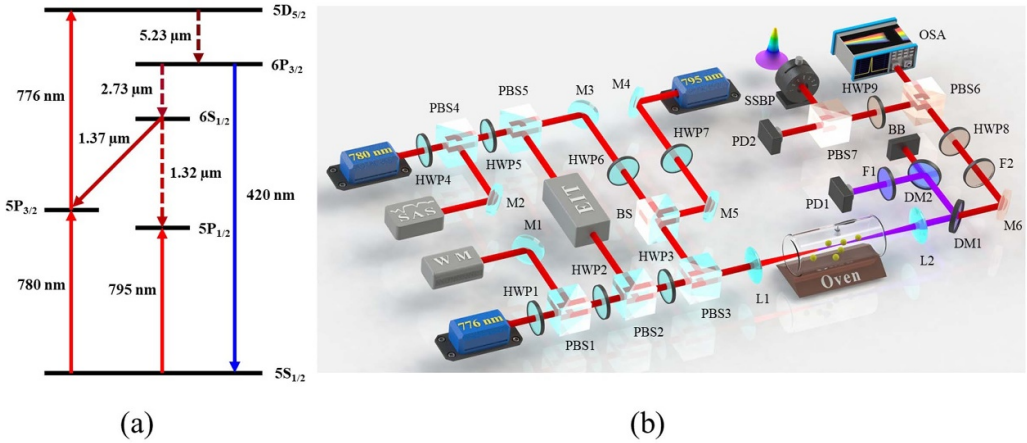

Figure 1. (a) Relevant energy levels in the experiment. (b) Schematic illustration of the experimental setup. HWP, half wave plate; PBS, polarization beam splitter; M, high reflection mirror; SAS, saturation absorption spectroscopy; EIT, electromagnetically induced transparency spectrum; WM, wavelength meter; L, lens; DM, dichroic mirror; PD, photodiode; BB, beam block; OSA, optical spectrum analyzer; SSBP, scanning slit beam profiler.

To date, coherent lights generated by the FWM in atomic mediums have been extensively investigated. The UV or blue emissions at 455 nm [17], 420 nm [18, 19], 311 nm [10], have been achieved in Rb or Cs vapors excited through two-photon excitation. However, the IR lights generated by FWM process in atomic ensembles have been rarely investigated owing to their low efficiency compared with UV or blue lights. The correlation between 780 nm and 1.37 μm photons are studied in Rb atomic ensemble [20, 21]. Then, the 1.37 μm coherent near-IR light (CNIRL) and 420 nm coherent blue light (CBL) have been simultaneously observed [11], and the major processes are also distinguished via orbital angular momentum transfer [22]. The interaction between ASE and FWM is demonstrated by IR and blue lights generated in Rb [23] or Cs [24] atomic systems. Therefore, in view of the outstanding advantages and possible applications in remote detection and other fields, a further research about generating high-quality and available IR laser is relevant.

In this paper, we report the CNIRL generation in dense Rb atomic vapor via ASE induced self-seeded FWM process. The generated coherent light wavelength is confirmed with an optical spectrum analyzer. The dependence of CNIRL power on various experimental parameters is investigated in detail, and the competition between two different parametric loops is clearly demonstrated. An additional 795 nm laser is used to increase the CNIRL output power through velocity-selective optical hyperfine repumping. This study is beneficial for understanding the FWM process in the atomic vapor cells. Furthermore, it provides an experimental basis for the light source used in laser guide star technique, remote magnetometry and long-distance quantum network.

2. Experiment setup

Figure 1(a) presents the multi-level structure of the FWM process. Two photons of 780 nm and 776 nm excite the Rb atoms from the $5S_{1/2}$ state to the $5D_{5/2}$ state. The cascade de-excitation of atoms is distributed among numerous paths, and induces multi-color ASE processes with population inversion. Then, these optical fields, which are generated internally via ASE processes, serve as seeded lights, inducing two different parametric loops under the two-photon excitation. Consequently, the 1.37 μm and 420 nm coherent lights are generated when the phase matching conditions are met.

Figure 1(b) schematically illustrates the experimental setup. The Rb atoms are excited stepwise from the $5S_{1/2}$ state to the $5D_{5/2}$ state using two pump lasers, which are provided by a 780 nm external cavity diode laser (DL pro, Toptica) and a 776 nm tapered amplifier diode laser (DLC TA pro, Toptica). The saturation absorption spectrum is used as the frequency reference for the 780 nm laser. The 776 nm laser frequency is referenced using an electromagnetically induced transparency spectrum in a reference cell and monitored by a wavelength meter (WS-7, High Finesse). The main strong beams consisting of 780 nm and 776 nm are overlapped with co-propagating configuration. A 5 cm long Rb vapor cell is used for the frequency conversion, which is housed in a μ-metal to shield stray magnetic field. The temperature is varied from 95 °C to 145 °C by a self-feedback system. The 1.37 μm and 420 nm coherent lights are generated with the occurrence of two parametric FWM processes. At present, the CBL has been widely studied [25], while the 1.37 μm CNIRL generated simultaneously is less efficient and difficult to be detected. Here, the 1.37 μm CNIRL is separated from the background light and blue light using a dichroic mirror and an IR filter, and simultaneously detected by the optical spectrum analyzer (AQ-6370C, ANDO) and IR photodiode (PDA20CS2, Thorlabs). The beam quality M^2 of the generated CNIRL is evaluated by using a scanning slit beam profiler (BP109-IR, Thorlabs). The 420 nm CBL is also detected with a photodiode (PDA36A-EC, Thorlabs).

3. Results and discussions

The wavelengths of the generated near-IR beams are detected using the optical spectrum analyzer, as shown in figure 2. The

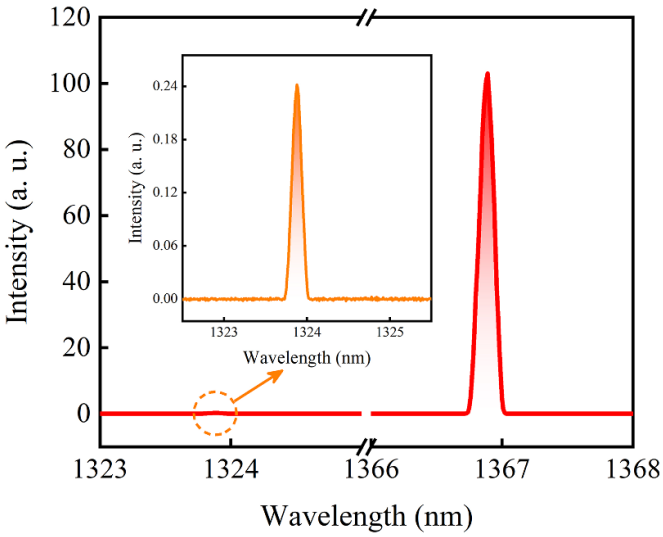

Figure 2. Signal of the output near-IR beam detected by an optical spectrum analyzer. The inset is the zoomed view of left peak.

frequency peak is centered at 1366.9 nm with the full-width at half-maximum of 0.13 nm corresponding to the $5P_{3/2}$–$5D_{5/2}$–$6P_{3/2}$–$6S_{1/2}$–$5P_{3/2}$ FWM process. While, the very weak peak in the left is centered at 1323.9 nm corresponding to the $6S_{1/2}$–$5P_{1/2}$ ASE process. The inset in figure 2 presents a zoomed view of the weak peak. The intensities of these two beams ($I_{1366.9\ \mathrm{nm}}/I_{1323.9\ \mathrm{nm}}$) have a large ratio, which exceeds the value of 400. Thus, we can consider that the detected signal represents the intensity of the 1366.9 nm CNIRL.

The competition between the two different parametric FWM loops shows interesting experimental results, characterized by the intensities of CNIRL and CBL. Figure 3 presents the concise two-dimensional maps of the CNIRL and CBL normalized intensities. The powers of the 780 nm and 776 nm lasers are 20 mW and 350 mW, respectively. The atomic density is approximately 1.51×10^{13} cm^{-3}. The resonance frequencies of the 780 nm and 776 nm lasers correspond to the hyperfine transitions of ^{85}Rb $5S_{1/2}$ ($F = 3$)–$5P_{3/2}$ ($F = 4$) and $5P_{3/2}$ ($F = 4$)–$5D_{5/2}$ ($F = 5$), respectively. The CNIRL is clearly observed around the ^{85}Rb $5S_{1/2}$ ($F = 2, 3$)–$5P_{3/2}$ and ^{87}Rb $5S_{1/2}$ ($F = 2$)–$5P_{3/2}$, while the CBL is detected only around the ^{85}Rb $5S_{1/2}$ ($F = 2, 3$)–$5P_{3/2}$. Moreover, the maximum intensities of CNIRL and CBL are achieved at different frequency positions. The maximum intensity of the 1.37 μm CNIRL is obtained when the two pump lasers resonate with ^{85}Rb $5S_{1/2}$ ($F = 3$)–$5P_{3/2}$ ($F = 4$)–$5D_{5/2}$ ($F = 5$), while the 420 nm CBL is relatively weak at this resonance position for the self-absorption effect [18, 25].

The clear competition between two different FWM processes of $5P_{3/2}$–$5D_{5/2}$–$6P_{3/2}$–$6S_{1/2}$–$5P_{3/2}$ and $5S_{1/2}$–$5P_{3/2}$–$5D_{5/2}$–$6P_{3/2}$–$5S_{1/2}$ leads to this result. To understand the competition between two self-seeded FWM processes start by ASE, the spontaneous decay rates of the involved different decay channels are given in [26]. The ASE process can be achieved only with the population inversion, which generates a directional optical field. Because $\Gamma_{5D_{5/2}-6P_{3/2}} < \Gamma_{6P_{3/2}-6S_{1/2}} < \Gamma_{6S_{1/2}-5P_{3/2}}$, substantial population inversions on the $5D_{5/2}$–$6P_{3/2}$ and $6P_{3/2}$–$6S_{1/2}$ transitions lead to the directional emissions at 5.23 μm and 2.73 μm. The two FWM loops of $5P_{3/2}$–$5D_{5/2}$–$6P_{3/2}$–$6S_{1/2}$–$5P_{3/2}$ and $5S_{1/2}$–$5P_{3/2}$–$5D_{5/2}$–$6P_{3/2}$–$5S_{1/2}$ are simultaneously established with the help of ASE processes. The former process generates the 1.37 μm CNIRL and the latter process produces the 420 nm CBL, their directions are determined by the phase matching conditions. Both processes originate from the de-excitation of the $5D_{5/2}$ state, which inevitably leads to competition between the two FWM processes. The result is beneficial for clearly understanding the underlying physics in such complex energy level structures and, thus enabling the realization of multi-wavelength lasers.

The CNIRL power depends on several experimental parameters, such as the input laser power and the atomic density. The CNIRL power dependence as a function of the 776 nm laser power is quantitatively investigated in figure 4(a). The two pump laser frequencies resonate with ^{85}Rb $5S_{1/2}$ ($F = 3$) –$5P_{3/2}$ ($F = 4$)–$5D_{5/2}$ ($F = 5$). The 780 nm laser power is 20 mW and the atomic density is about 7.85×10^{13} cm^{-3}. The frequency conversion efficiency dramatically increases when the applied laser power is less than 220 mW. Further, the saturation of the CNIRL power is observed as the 776 nm input power continues to increase. This behavior is expected because the two optical fields involved in the parametric FWM process originate from the ASE processes and should possess threshold-like power dependence [11]. For the given input laser powers of 20 mW and 350 mW, figure 4(b) shows the CNIRL power versus atomic density ranging from 4.34×10^{12} cm^{-3} to 7.85×10^{13} cm^{-3}. A threshold dependence on the atomic density is observed, in other words, a sufficiently large atomic density is required to start the FWM process. The CNIRL power steadily and linearly increases as the atomic density increases, without noticeable saturation.

In order to evaluate beam quality of the CNIRL, the beam profile is directly measured, as shown in the inset of figure 5. A good Gaussian beam profile is clearly demonstrated. The two pump laser frequencies resonate with ^{85}Rb $5S_{1/2}$ ($F = 3$) –$5P_{3/2}$ ($F = 4$)–$5D_{5/2}$ ($F = 5$) transitions and the powers are 20 mW and 350 mW. The atomic density is approximately 7.85×10^{13} cm^{-3}. In figure 5, the measured beam waists at different positions along the x axis and y axis, are represented by black squares and red circles, respectively. The resulting M^2 values are $M_x^2 = 1.22$ and $M_y^2 = 1.25$. Thus, the novel coherent light generated in an atomic medium also shows a good beam profile with respect to the crystal case [27].

Velocity-selective optical hyperfine repumping can significantly enhance the efficiency of the parametric FWM process [18]. The population of the $5S_{1/2}$ ($F = 3$) state can be enhanced using an additional laser interacting with the $5S_{1/2}$ ($F = 2$) state. Figure 6(a) shows the enhancement effect with a repump laser resonating with $5S_{1/2}$ ($F = 2$)–$5P_{1/2}$ transition. The inset presents a zoomed view of the weak peak. The related experimental parameters are similar to those of figure 5, and the 795 nm repump laser power is 21 mW. As a result, the maximum power of the 1.37 μm CNIRL is improved by a factor of approximately 1.5, while the 1.32 μm beam

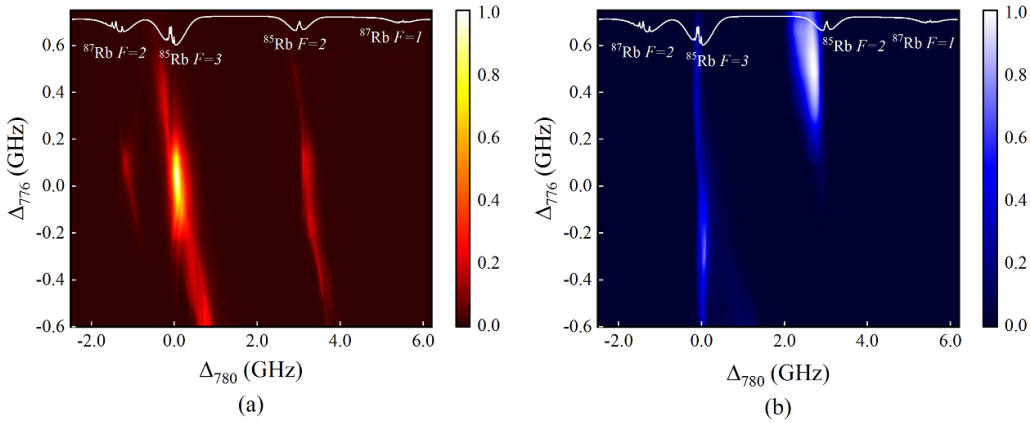

Figure 3. Normalized intensities of (a) CNIRL and (b) CBL as a function of the two pump laser frequencies. The white curve denotes the saturated absorption spectrum (SAS) of 780 nm laser.

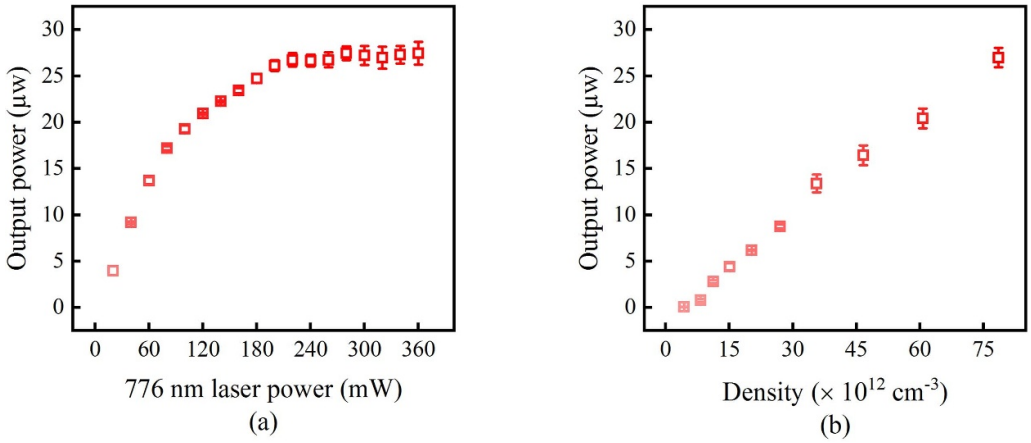

Figure 4. Generated CNIRL power versus (a) 776 nm laser power and (b) atomic density. The error represents the standard deviation of three measurements.

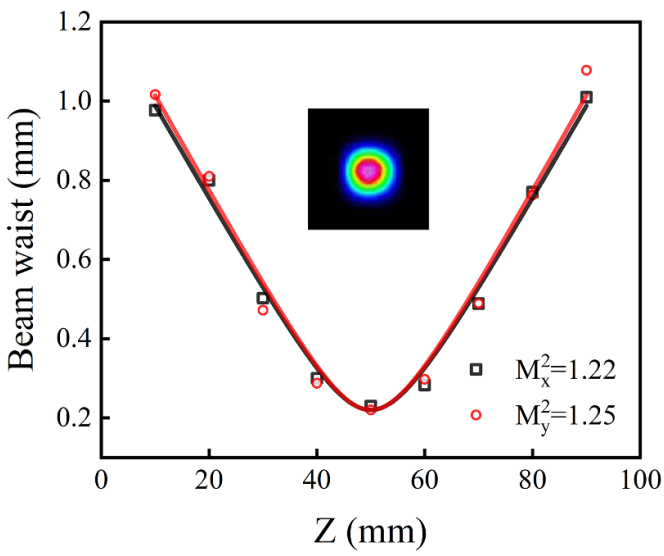

Figure 5. The measured beam quality M^2 of the output CNIRL. The black squares and red circles represent the experimental data on the x axis and y axis, respectively. The insert shows the CNIRL profile.

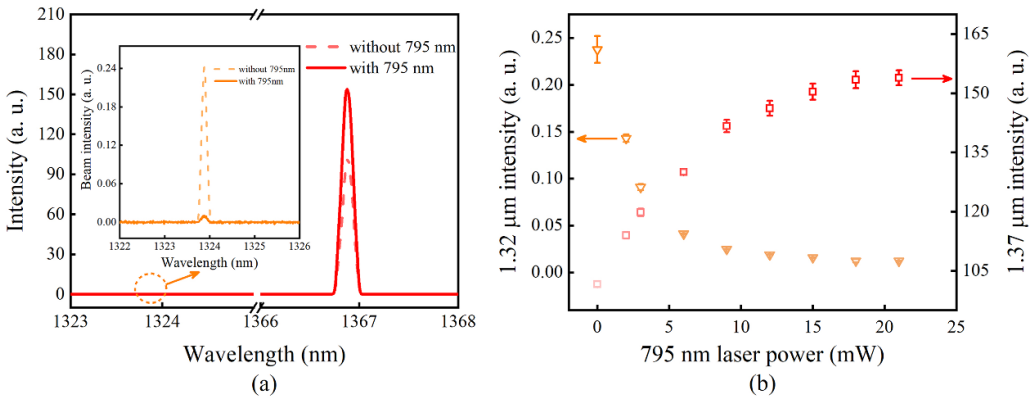

Figure 6. (a) Intensities of the generated 1.37 μm and 1.32 μm beams with or without the 795 nm repump laser. The inset shows the zoomed view of the left peak. (b) Intensities of the generated 1.37 μm and 1.32 μm beams as a function of the repump laser power. The error represents the standard deviation of three measurements.

is completely suppressed due to population increase in the $5P_{1/2}$ state. Figure 6(b) shows the dependence of the generated 1.37 μm and 1.32 μm beams on the repump laser power. The conversion efficiency of the FWM process dramatically increases as the applied repump laser power increases.

4. Conclusions

In summary, the CNIRL at 1.37 μm is experimentally generated in Rb vapor via ASE induced self-seeded FWM process. The spectral and spatial characteristics of CNIRL are investigated in detail. The maximum intensities of CNIRL and CBL occur at the different frequency positions, the result clearly shows the competition between the two different FWM processes. Under the optimal experimental parameters, a 27 μW CNIRL with the beam quality of $M_x^2 = 1.22$ and $M_y^2 = 1.25$ is obtained. Additionally, the output power is further enhanced by a factor of approximately 1.5 by introducing a 795 nm repump laser. In future work, the circulating intensity of the two-photon excitation beam can be increased using an external cavity. The approach used herein is applicable to various atomic media, and inherently suitable for developing polychromatic, coherent and frequency tunable lasers.

Acknowledgments

This work is supported by the National Key Research and Development Program of China (2017YFA0304203); National Natural Science Foundation of China (61875112, 62075121, and 91736209); Program for Sanjin Scholars of Shanxi Province; Key Research and Development Program of Shanxi Province for International Cooperation (201803D421034); Research Project Supported by Shanxi Scholarship Council of China under Grant Nos. 2020-073 and 1331KSC.

References

[1] Pitz G A and Anderson M D 2017 *Appl. Phys. Rev.* **4** 04110
[2] Biswal R, Mishra G K, Agrawal S K, Dixit S K and Nakhe S V 2019 *Pramana J. Phys.* **93** 58
[3] Ding D S, Zhou Z Y, Shi B S, Zou X B and Guo G C 2012 *Opt. Express* **20** 11433
[4] Yuan J P, Dong S C, Wu C H, Wang L R, Xiao L T and Jia S T 2020 *Opt. Express* **28** 23820
[5] Gao W B, Imamoglu A, Bernien H and Hanson R 2015 *Nat. Photon.* **9** 363
[6] Yuan J P, Wu C H, Wang L R, Chen G and Jia S T 2019 *Opt. Lett.* **44** 4123
[7] Li C H, Li W, Zhang D, Zhang Z Y, Gu B L, Li K K and Zhang Y P 2020 *Laser Phys. Lett.* **17** 015401
[8] Zibrov A S, Lukin M D, Hollberg L and Scully M O 2002 *Phys. Rev.* A **65** 051081
[9] Antypas D, Tretiak O, Budker D and Akulshin A 2019 *Opt. Lett.* **44** 3657
[10] Lam M, Pal S B, Vogt T, Gross C, Kiffner M and Li W H 2019 *Opt. Lett.* **44** 2931
[11] Akulshin A, Budker D and McLean R 2014 *Opt. Lett.* **39** 845
[12] Raymond C S and Karen S B 1981 *Appl. Opt.* **20** 177
[13] Happer W, MacDonald G J, Max C E and Dyson F J 1994 *J. Opt. Soc. Am.* A **11** 263
[14] Bustos F P, Calia D B, Budker D, Centrone M, Hellemeier J, Hickson P, Holzlohner R and Rochester S 2018 *Nat. Commun.* **9** 3981
[15] Akulshin A M, Bustos F P and Budker D 2018 *Opt. Lett.* **43** 5279
[16] Covey J P, Sipahigil A and Saffman M 2019 *Phys. Rev.* A **100** 012307
[17] Schultz J T, Abend S, Döring D, Debs J E, Altin P A, White J D, Robins N P and Close J D 2009 *Opt. Lett.* **34** 2321
[18] Vernier A, Franke-Arnold S, Riis E and Arnold A S 2010 *Opt. Express* **18** 17020
[19] Akulshin A M, Orel A A and McLean R J 2012 *J. Phys. B: At. Mol. Opt. Phys.* **45** 015401
[20] Willis R T, Becerra F E, Orozco L A and Rolston S L 2010 *Phys. Rev.* A **82** 053842
[21] Willis R T, Becerra F E, Orozco L A and Rolston S L 2011 *Opt. Express* **19** 14632
[22] Akulshin A M, McLean R J, Mikhailov E E and Novikova I 2015 *Opt. Lett.* **40** 1109
[23] Sebbag Y, Barash Y and Levy U 2019 *Opt. Lett.* **44** 971
[24] Zhang Y Y, Wu J, He Y Y, Zhang Y, Hu Y D, Zhang J X and Zhu S Y 2020 *Opt. Express* **28** 17723
[25] Liu H, Yuan J P, Wang L R, Xiao L T and Jia S T 2020 *Chin. Phys.* B **29** 043203
[26] Heaven O S 1964 *J. Opt. Soc. Am.* **51** 1058
[27] Akbari R and Major A 2013 *Laser Phys.* **23** 035401